



# Thermal, dielectric, mechanical and structural behavior of 2-amino 4-methylpyridinium 4-nitrophenolate 4-nitrophenol bulk single crystal

S. Karuppusamy<sup>a,b</sup>, S. Muralidharan<sup>a</sup>, K. Dinesh Babu<sup>a,c</sup>, P. Sakthivel<sup>d,\*</sup>, Dongjin Choi<sup>e,\*\*</sup>

<sup>a</sup> Crystal Research Laboratory, Department of Physics, Anna University, Chennai, 600 025, Tamil Nadu, India

<sup>b</sup> Department of Physics, Excel Engineering College (Autonomous), Komarapalayam 637303, Tamil Nadu, India

<sup>c</sup> Department of Electrical and Electronics Engineering, Sri Shakthi Institute of Engineering and Technology, Coimbatore, 641 062, Tamil Nadu, India

<sup>d</sup> Centre for Materials Science, Department of Physics, Science and Humanities, Faculty of Engineering, Karpagam Academy of Higher Education, Coimbatore, 641 021, Tamil Nadu, India

<sup>e</sup> Department of Materials Science and Engineering, Hongik University, 2639-Sejong-ro, Jochiwon-eup, Sejong-city, 30016, South Korea

## ARTICLE INFO

### Keywords:

2-Amino 4-methylpyridinium 4-nitrophenolate  
4-nitrophenol crystal  
Vertical Bridgman technique  
FTIR  
Dielectric parameters  
Thermal kinetics  
Vickers hardness number

## ABSTRACT

Applications in both science and industry have received increased attention as a result of bulk single crystals with particular orientations. However, due to the instability of organic crystals at high temperatures and stress, there is an interest in growing good-quality bulk single crystals with stable thermal and mechanical properties. Here, the 2-amino 4-methylpyridinium 4-nitrophenolate 4-nitrophenol (2A4MPPP) crystal was prepared employing a single-wall ampoule and the vertical Bridgman technique. Structure and functional groups were determined by XRD, NMR, and FTIR studies. More importantly, detailed thermal and kinetic properties such as activation energy, frequency factor, rate constant, and Avrami exponent are discussed. The mechanical stability and dielectric studies are also demonstrated for the title compound. According to the single crystal XRD investigation, 2A4MPPP is a member of the orthorhombic crystal system with the Pna21 space group. Through the TGA and DTA analyses, it was confirmed that the compound starts to melt at 98 °C and complete melting occurs at 103.3 °C. The dielectric experiments reveal the crystal's poor dielectric constant and high-frequency dielectric loss. Vickers microhardness investigations show that grown 2A4MPPP belongs to the soft materials group. As a result of these findings, the 2A4MPPP crystal should be well suited for usage in thermomechanical, microelectronic, optical communications, and nonlinear optical applications.

## 1. Introduction

The best prospects for exposing a material's intrinsic qualities are single crystals. Organic bulk crystalline materials with specific orientations [1,2] have attracted more attention in micro-electronics, thermoelectrics, optical communications, optoelectronics and scintillators [3–6]. The economy, simple synthesis routes and easy structural modifications of organic crystals have made them suitable

\* Corresponding author.

\*\* Corresponding author.

E-mail addresses: [sakthi1807@gmail.com](mailto:sakthi1807@gmail.com) (P. Sakthivel), [djchoi@honigk.ac.kr](mailto:djchoi@honigk.ac.kr) (D. Choi).

<https://doi.org/10.1016/j.heliyon.2023.e18260>

Received 8 May 2023; Received in revised form 7 July 2023; Accepted 12 July 2023

Available online 13 July 2023

2405-8440/© 2023 The Authors. Published by Elsevier Ltd. This is an open access article under the CC BY-NC-ND license (<http://creativecommons.org/licenses/by-nc-nd/4.0/>).

for industrial applications. Organically mixed crystals of phenol-pyridine and phenol-amine compounds have proven to be outstanding materials for nonlinear optical device applications [7]. It has been shown that the ionic interaction between the anion of 4-nitrophenol and the cation of a pyridine compound increased  $\pi$ -delocalization and several  $\pi$  electrons, which results in enhanced second-order nonlinearity and high-frequency conversion efficiency compared to standard materials such as KDP and urea. However, these applications require bulk single crystals without defects or impurities.

The vertical Bridgman technique is one of the most well-known and conventional techniques to grow void- and crack-free bulk single crystals with a desired orientation. The growth of crystals using the Bridgman technique can be performed either vertically or horizontally [8–12], where the seed crystal is grown using specially designed conical ampoules [13]. Though the solution growth method has been known for several years, many difficulties, such as solvent inclusion and defects severely affecting stability, still need

**Table 1**

Comparison analysis of thermal, mechanical and dielectric properties of various crystal structures.

S.NO	Details of material prepared	Findings	Author name	Reference
1	By using the traditional solid-state process, LiCoO <sub>2</sub> formed.	AC conductivity value measured ( $10^{-4} \Omega^{-1} \text{cm}^{-1}$ ). By examining the temperature dependence of the electrical characteristics, it was demonstrated that the exothermic peak of the thermal analysis occurs at 335 K.	I.B. Slima et al.	[20]
2	Organic-inorganic compound Penta-dimethylammonium-Undecachlorotricadmate (II) [(CH <sub>3</sub> ) <sub>2</sub> NH <sub>2</sub> ] <sub>5</sub> Cd <sub>3</sub> Cl <sub>11</sub> hybrid material prepared by classic evaporation method at room temperature.	The properties of thermal, vibrational, optical, and electrical systems were examined.	K. Trabelsi et al.	[21]
3	A solid-state technique was used to create NaCu <sub>0.2</sub> Fe <sub>0.3</sub> Mn <sub>0.5</sub> O <sub>2</sub> with a hexagonal form.	Using complex impedance spectroscopy between 101 Hz and 106 Hz at various temperatures (333–453 K), the material's electrical and dielectric characteristics were examined.	I.B. Slima et al.	[22]
4	2-amino-4,6-dimethylpyrimidine 4-nitrophenol (AMP4N) single crystals are grown by slow evaporation solution technique	Studies on third-order nonlinear optics, thermal analysis, and chemical etching were conducted. The AMP4N crystal was proven to be thermally stable up to 120 °C by TG-DTA experiments.	P. Karuppusamy et al.	[23]
5	Monoclinic structured 2-Amino 4-methylpyridinium 3-chlorobenzoate (2A4M3CB) synthesized using slow evaporation solution growth technique	TGA and DTA thermograms validated 2A4M3CB's stability up until its melting point, which was determined to be 184 °C. Vickers Micro Hardness Tester analysis of the crystals' mechanical strength reveals that 2A4M3CB exhibits a reversal indentation size effect.	B. Babu et al.	[24]
6	hexamethylenetetramine 4-nitrophenol monohydrate (HMTNP) solvent evaporation method was used	Tests for photoconductivity, second harmonic generation, and dielectric were done. The lower dielectric constant ( $\epsilon_r$ ) of the HMTNP crystal is 9.516 at 393 K.	M. Saravanakumar et al.	[25]
7	monoclinic crystal 2-amino-6-methylpyridinium 2,4-dihydroxybenzoate monohydrate (2A6MDH) organic single crystal was grown by slow evaporation method	The 2A6MDH crystal was discovered to have a thermal stability of 77.8 °C. The generated crystal was a soft category material according to Vickers' hardness examination, suggested for optoelectronic applications.	R. Kaliammal et al.	[26]
8	2-Amino-4-methylpyridinium 2-chloro 4-nitro benzoate (AMPNCB) was synthesized by slow evaporation solution growth method.	The results of a micro-hardness analysis showed that the produced crystals are soft mechanically. Lower dielectric constant readings at higher frequencies indicated that the crystal included less electrically active flaws.	K. Venkatesan et al.	[27]
9	2-amino 5-methylpyridinium 4-methoxybenzoate (2A5MP4MB) have been grown successfully from the aqueous solution by slow evaporation technique.	Received greater thermal stability at 178 °C without deterioration and crystallization of water. Dielectric analysis demonstrated the crystal's typical optical behaviour for photonic applications. According to a microhardness investigation, 2A5MP4MB crystal was a soft material.	T. Murugan et al.	[28]
10	2,3-Dimethyl-N-[2-(hydroxy) benzylidene] aniline (DHBA) using slow evaporation solution growth method in methanol.	The results of the TG/DTA investigation showed that DHBA was thermally stable up to 197 °C. The DHBA had good crystal quality with fewer flaws due to the low amount of dielectric constant/dielectric loss at high frequencies. According to the Vickers microhardness test, the formed crystal had category of soft materials.	B.R. Krishnamoorthy	[29]
11	Triclinic bis(2-amino-6-methyl pyridinium barbiturate) tetrahydrate (2A6MBA) has been grown as a single crystal by slow evaporation solution growth method	The TG-DSC research verified that the material was thermally and chemically stable up to 103.9 °C and that no phase transformation had occurred. Vicker's microhardness demonstrated the crystal's mechanical stability, and the hardness number was computed using several models, while the etching research showed the crystal's flawless structural reliability.	R. Kaliammal et al.	[30]

to be overcome. Recently, the synthesis, growth and fundamental characterization of mixed crystals of phenol-pyridine and phenol-amine compounds by the slow evaporation solution growth method have been reported [14–19]. However, no reports are available on melt growth methods for these crystals. A comparison analysis of the thermal, mechanical and dielectric properties of various crystal structures is given in Table 1.

In this study, bulk single-crystal growth of 2-amino 4-methyl pyridinium 4-nitrophenolate 4-nitrophenol (2A4MPPP) was reported. This growth was achieved using the vertical Bridgman technique and a single wall ampoule, which was found to satisfy the growth conditions from the melt and have good thermal stability. The vertical Bridgman approach was used to effectively develop a sizable, high-quality 2A4MPPP crystal, and this achievement has been disclosed to the scientific community for the first time. The homemade Bridgman system's instrumentation and the ampoule's measured cone angle have been presented. The Physical, chemical, dielectric and mechanical properties of 2A4MPPP crystal have also been investigated using single crystal XRD, powder XRD, 1H.NMR, FTIR, TG-DTA, dielectric studies, Vicker's microhardness test, and the results have been discussed in detail. By the Kissinger and Ozawa method [31], thermal kinetic parameters were evaluated and from the Arrhenius equation, the thermal and electrical activation energies of the title compound were calculated.

## 2. Experimental details

### 2.1. Design of Bridgman growth system

To grow bulk crystal, a single-zone transparent vertical furnace made of borosilicate glass and a new homemade Bridgman system with various components such as a heating element, temperature controller, thermocouple, thyristor, and crystal puller with control system were designed. Fig. 1 depicts the Bridgman system's schematic representation. With the crystal pulling system, a stepper motor with a lead screw was used to regulate the ampoule's vertical position inside the furnace. An additional control system managed the speed of the stepper motor to optimize the growth rate. Organic compounds generally require a low translation rate due to their poor thermal conductivity [32,33] and low growth rate to grow into good-quality single crystals. Hence, the translation speed was cautiously optimized to 0.4–0.5 mm/h, where a solid-liquid interface of concave shape was observed. One can also achieve a planar or convex interface by changing the translation speed and width of the ampoule [34]. A detailed numerical simulation model of organic materials can better understand the interface's nature, growth process, and formation of cracks. However, such simulations involve many experimental parameters such as viscosity, the flow velocity of the melt, gravitational force, and thermal conductivity of the sample, as well as ampoule design [35,36].

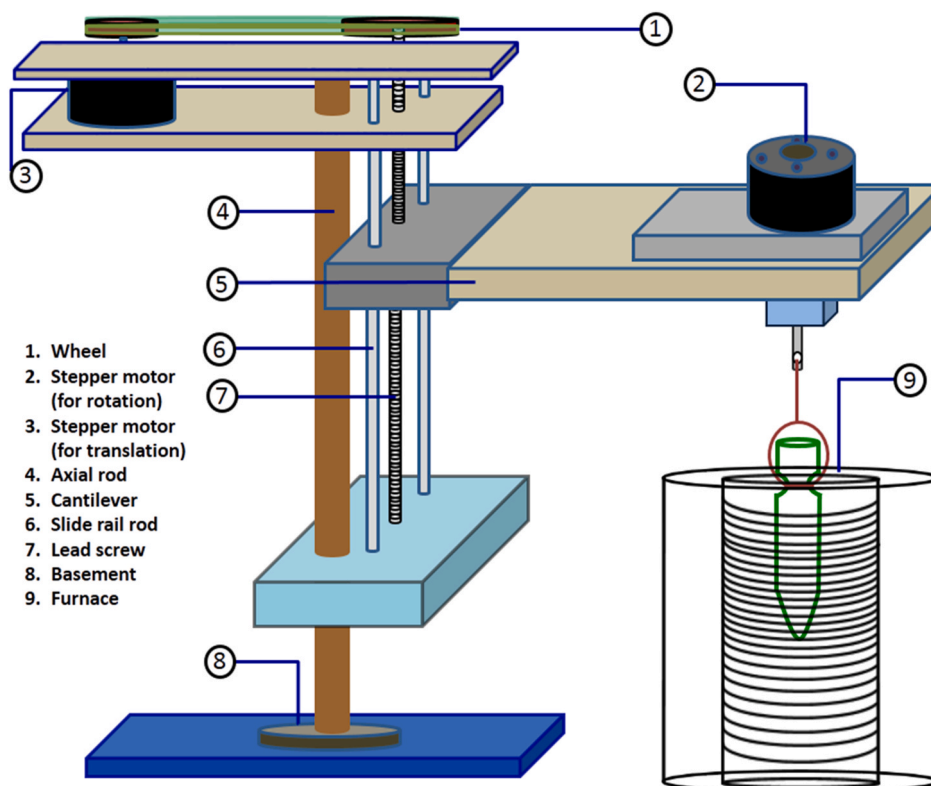


Fig. 1. Schematic diagram of Bridgman crystal puller setup with furnace.

Furnace heating can be done in two ways, resistive and inductive heating [37]. The resistive heating method is inexpensive and efficient for temperature optimization. Hence, the resistive heating method using a stripe type A1 grade kanthal wire was followed in the growth process. The furnace temperature was fully controlled with a Eurotherm temperature controller (model no.: 3216) and thyristor (model no.: 7100). A proportional integral differential (PID) controller was used to create the furnace's precise and targeted temperature profile. The schematic picture of the furnace setup and its optimized temperature profile is shown in Figs. 2 and 3.

## 2.2. Ampoule

Ampoule design and cone angles are the main factors that influence the formation of nucleation and the quality of single crystals from melt. Therefore, a single-walled borosilicate ampoule of length 150 mm, diameter 12 mm and perpendicular length of cone 40 mm was designed. The measured cone angles were  $17^{\circ}2'$  at the bottom tip and  $171^{\circ}28'$  at the neck position. The schematic diagram of the ampoule with its cone angle is illustrated in Fig. 4. While choosing the ampoule, chemical reactivity and thermal stability with the 2A4MPPP compound were checked. The ampoule was completely cleaned with the soap solution, thoroughly washed with de-ionized water, and then soaked in ethanol to eliminate contaminants inside. The cleaned ampoule was then thoroughly dried at  $80^{\circ}\text{C}$ .

## 2.3. Sample preparation

In 200 ml of ethanol solvent, highly pure 2-amino-4-methylpyridine and 4-nitrophenol compounds were combined in a 1:2 ratio. To completely dissolve the compounds, the solution was thoroughly agitated for 5 h. Afterward, it was filtered through Whatman filter paper to get rid of any indissoluble particles and contaminants. The filtered solution evaporated at  $40^{\circ}\text{C}$  in a constant-temperature bath. The reaction was depicted as per the scheme represented in Fig. 5. The 2-amino 4-methylpyridinium cation interacts with the 4-nitrophenolate anion and neutral 4-nitrophenol stands as another partner; hence 2A4MPPP crystal was formed. The excellent quality crystals were harvested over 5 days and ground well into fine powder samples to load into the ampoule.

## 2.4. Growth process

The optimized temperature profile of the furnace was used to grow the bulk single crystal. By changing the lowering rate of the ampoule, a perfect growth atmosphere was provided for the compound. The furnace temperature was kept slightly above its melting temperature to attain a homogeneous melt without air bubbles. When the ampoule was lowered at a rate of 0.4–0.5 mm/h, the polycrystalline powder sample started to melt at its melting point; subsequently, supercooling was achieved. Nucleation started when the tip of the ampoule reached the crystallization point of 2A4MPPP, and the solidification process continued till all molten charges were converted to a single bulk crystal. It also ensured that the single crystal grown attained a particular orientation. To prevent the growth of crystal cracks, the furnace was progressively cooled down to room temperature after the melt-to-crystal conversion. The ampoule's developed crystal of 2A4MPPP was removed by cutting it using a diamond cutter (Fig. 6).

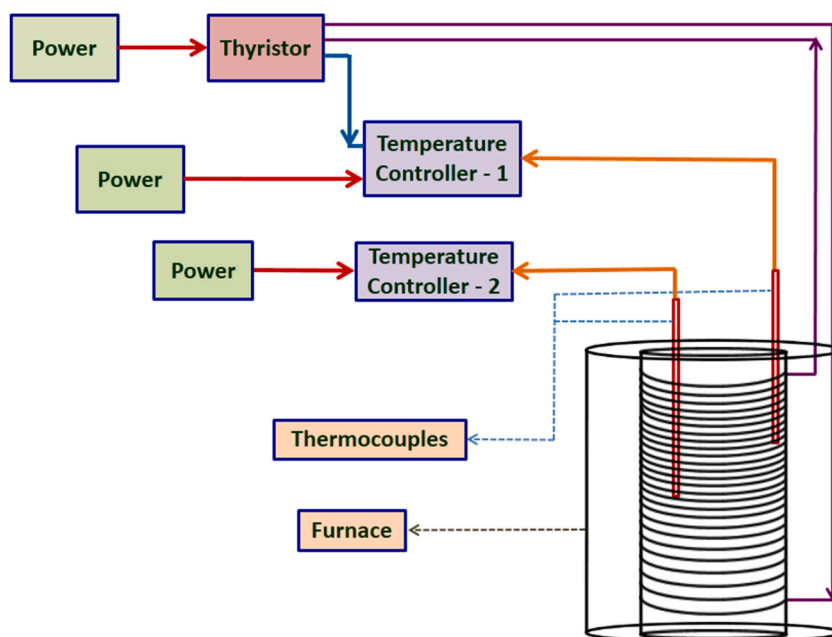


Fig. 2. Schematic diagram of furnace with temperature control system.

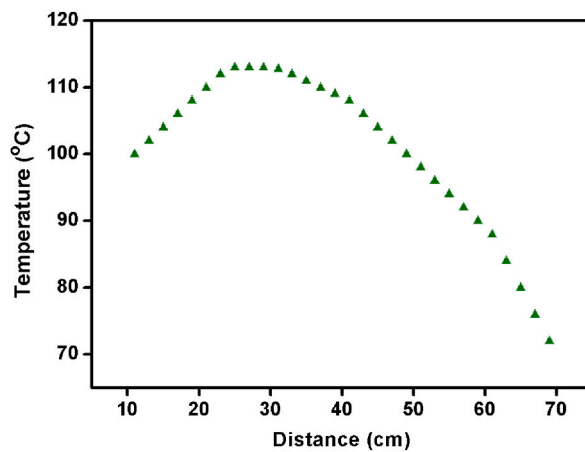


Fig. 3. Temperature profile of the furnace.

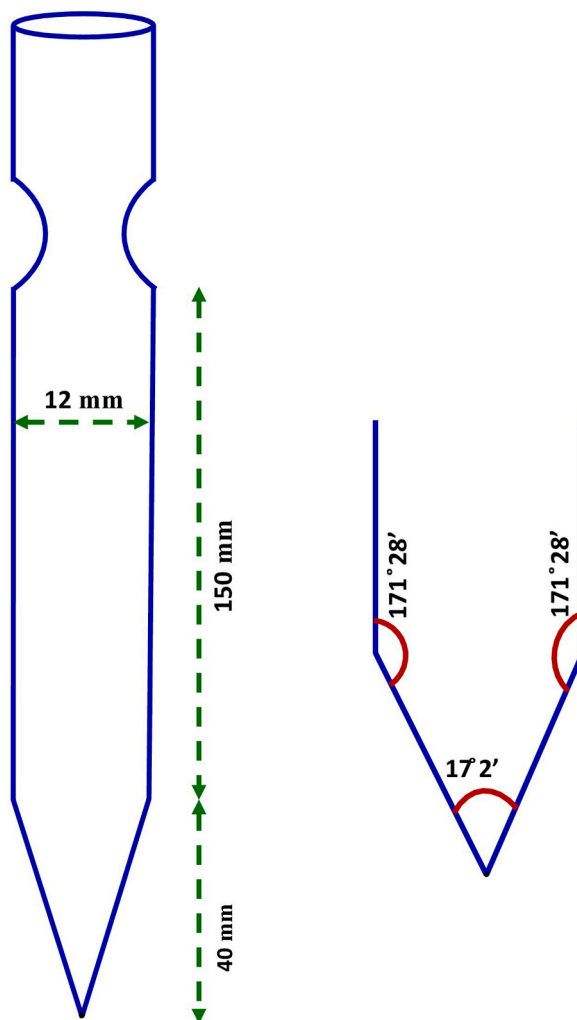


Fig. 4. Schematic diagram of ampoule with cone angle.

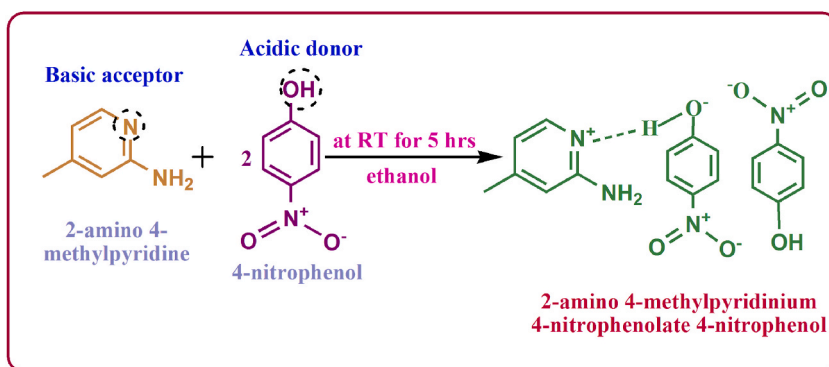


Fig. 5. Reaction scheme of 2A4MPPP crystal.



Fig. 6. The Bulk single crystal of 2-amino 4-methylpyridinium 4-nitrophenolate 4-nitrophenol grown by VBT.

## 2.5. Characterization studies

A single crystal X-ray diffractometer called the Bruker AXS Kappa APEX-II was used to examine the lattice parameters and space group of the title chemical at ambient temperature. The BRUKER D2 PHASER equipment was also used to do powder-XRD tests. For measurements in the 10–70° range, CuK radiation (1.5406 Å) was employed with a scanning rate of 0.02°/S. The 1H confirms the 2A4MPPP crystal's chemical composition. Utilizing a BRUKER ADVANCE-III 500 MHz spectrometer, NMR spectra were obtained using deuterated methanol as the solvent. Using Bruker ALPHA in KBr pellet mode, the FTIR spectra of 2A4MPPP were captured between 500 and 4000  $\text{cm}^{-1}$ . Using a HITACHI-STA-7300 instrument, the thermal stability of 2A4MPPP was examined between ambient temperature and 400 °C. TG-DTA found thermal kinetic parameters at various heating rates. A parallel plate capacitor was formed using the silver-coated <010> -oriented 2A4MPPP crystal with a dimension of  $8.09 \times 5.63 \times 1.87 \text{ mm}^3$  as the dielectric in between a pair of copper electrodes, and dielectric measurements were carried out using HIOKI 3532-50 LCR HITESTER. The applied frequency varied from 50 Hz to 5 MHz, and the capacitance values were noted at various temperatures like 40, 50, 60, 70 and 80 °C. The MATSUZAWA MMT-X instrument checked the mechanical hardness. The crystal was subjected to Vicker's hardness tester for an applied load ranging from 1 to 100 g at room temperature for <010> orientation of the crystal.

## 3. Results and discussion

### 3.1. X-ray diffraction

The orthorhombic space group Pna21 is the origin of the 2A4MPPP crystal, according to single crystal X-ray diffraction. The values of lattice parameters and volume are measured to be  $a = 13.175 \text{ \AA}$ ,  $b = 11.889 \text{ \AA}$ ,  $c = 12.052 \text{ \AA}$ , and  $V = 1877 \text{ \AA}^3$ , respectively. These values agree with the previously reported values [38]. The powder-XRD pattern of 2A4MPPP is depicted in Fig. 7. The plane of the title compound has been indexed using the powder-X software.

### 3.2. NMR spectral studies

The proton NMR spectrum of the title compound is depicted in Fig. 8. The peak at 7.73 ppm indicates the presence of the pyridinium ring. The doublet at 8.11 ppm is attributed to the NH formation of the pyridinium ring with 4-nitrophenol. The sharp, intense peak at 5.0 ppm is due to aromatic C-OH. The multiple peaks observed at 6.87 ppm are ascribed to the benzene ring's CH. The formation of hydrogen bonds between 2 - amino 4 - methylpyridine and 4-nitrophenol compounds accounts for the slight change in the chemical environment, which modifies the chemical shift. The 2A4MPPP crystal's molecular structure was validated based on the above examination of chemical shift data.

### 3.3. FTIR spectral studies

The FTIR spectrum of the 2A4MPPP crystal is depicted in Fig. 9. The peak at  $3427 \text{ cm}^{-1}$  is ascribed to O–H vibration. The slight shift of this frequency from the usual range  $3640\text{--}3610 \text{ cm}^{-1}$  could be explained by the presence of O–H of 4-nitrophenol or protonated N–H of 2-amino 4-methylpyridinium. The asymmetric vibration of  $\text{NH}_2$  is attributed to the peak seen at  $3337 \text{ cm}^{-1}$ . The aromatic ring's C–H stretching is responsible for the peak that was visible at  $3098 \text{ cm}^{-1}$ . At 2892 and  $2806 \text{ cm}^{-1}$ , the  $\text{CH}_3$  group's stretching vibrations are both symmetric and asymmetric. A band received near  $2586 \text{ cm}^{-1}$  is indexed to OH stretching vibrations of the acid group [26]. The peaks observed at 1668 and  $1625 \text{ cm}^{-1}$  are attributed to the vibration of the pyridine ring of 2-methyl 4-aminopyridinium. The ring

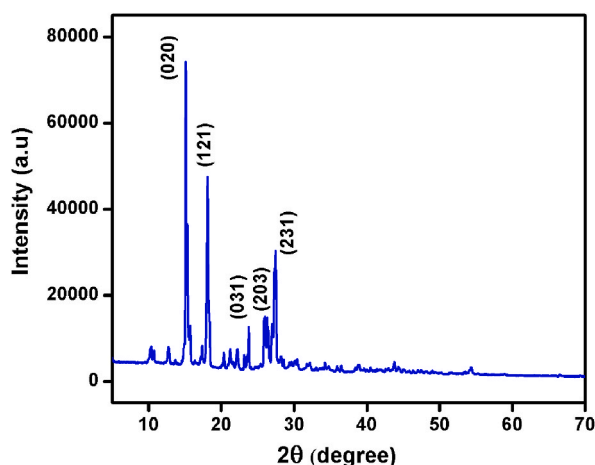


Fig. 7. Powder - XRD pattern of 2A4MPPP.

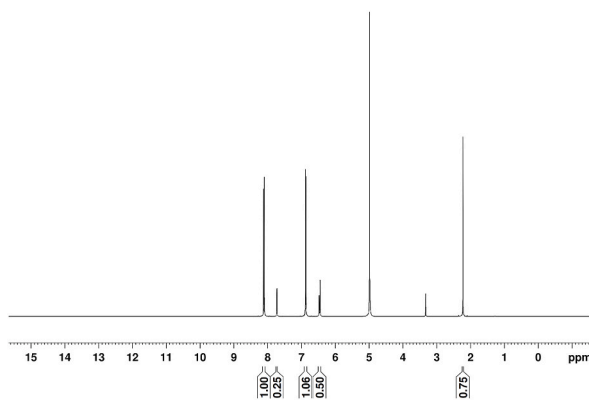


Fig. 8. Proton NMR spectrum of 2A4MPPP.

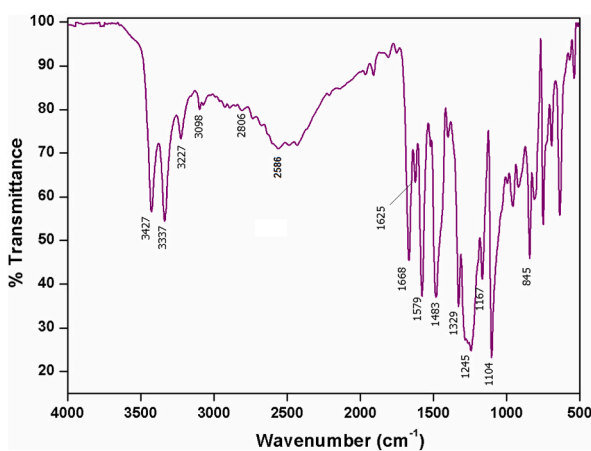


Fig. 9. FTIR spectrum of 2A4MPPP.

vibration of 4-nitrophenol is confirmed at 1483 and 1579  $\text{cm}^{-1}$ . The C–N stretching vibrational peak is identified at 1329  $\text{cm}^{-1}$ . The strong peak obtained at 1245  $\text{cm}^{-1}$  indicates the presence of the C–O stretching vibration of substituted phenol. The peak shift could be the electron-withdrawing ability of nitrogen in pyridine from the phenol group of 4-nitrophenol, which also results in the nonlinearity of the phenolate ion in 2A4MPPP. The presence of peaks at 1167, 1104 and 961  $\text{cm}^{-1}$  are ascribed to in-plane bending mode vibration modes of aromatic C–H. The band at 845  $\text{cm}^{-1}$  represents the vibration of the C–N–C inplane bending mode of the pyridine ring. The peaks observed at 755 and 544  $\text{cm}^{-1}$  are assigned to  $\text{NO}_2$  scissoring mode and rocking vibration, respectively. The intermolecular charge transfer between 2-amino 4-methylpyridine and 4-nitrophenol causes the downshift in wavenumber and validates the significant nonlinear optical activity of the material.

### 3.4. Thermal studies

The TG-DTA curve of 2A4MPPP is shown in Fig. 10(a). The TG curve indicates no weight loss from room temperature to 145  $^{\circ}\text{C}$  for the title compound. The weight loss starts at 145  $^{\circ}\text{C}$  and gradually increases up to 250  $^{\circ}\text{C}$  where it almost decomposes. The compound starts to melt at 98  $^{\circ}\text{C}$  and complete melting occurs at 103.3  $^{\circ}\text{C}$ , corresponding to the title compound's melting point. A sharp endothermic peak at 103.3  $^{\circ}\text{C}$  in the DTA curve confirms this. In the TG curve, no peaks are observed before the melting point, which confirms the absence of solvent inclusion in this compound. Hence, the 2A4MPPP crystal can potentially be exploited for any application up to 98  $^{\circ}\text{C}$ .

The thermal kinetic parameters are vital in understanding the nucleation process, growth transformation's kinetics, and reaction order. Furthermore, these data can prevent hazardous reactions [39]. Based on the Avrami equation [40], Avrami exponent ( $n$ ) at different heating rates, activation energy ( $E_a$ ), rate constant ( $K$ ) and frequency factor ( $K_0$ ) were calculated through the Arrhenius equation as per Equation (1).

$$K = K_0 \exp\left(\frac{-E_a}{RT_m}\right) \quad (1)$$

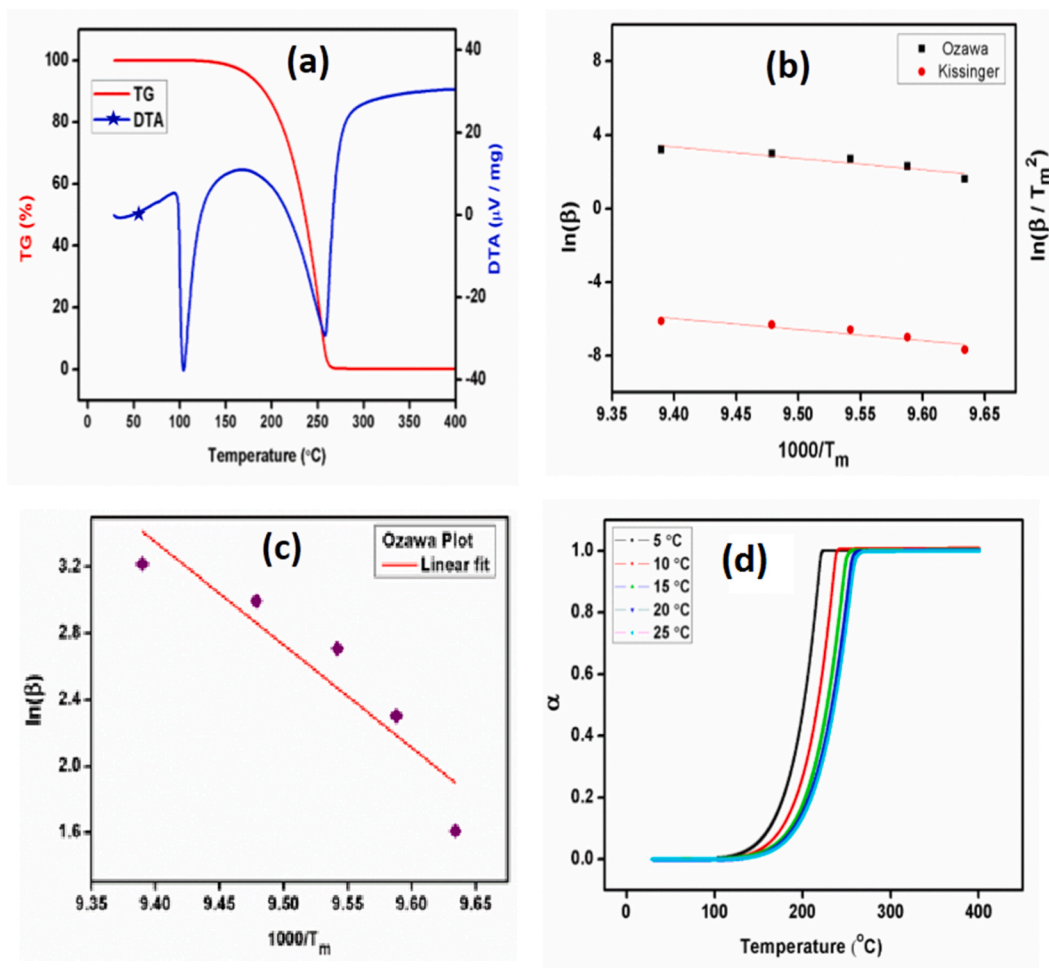


Fig. 10. (a) TG-DTA curve of 2A4MPPP at heating rate of 10 °C, (b) Kissinger plot, (c) Ozawa plot, (d) Plot between  $\alpha$  and Temperature.

where  $R$  is the real gas constant and  $T_m$  is the compound's melting point. At the melting point of the DTA curve, the activation energy and frequency factor were calculated using the Kissinger and Ozawa equations given in Equations (2) and (3) [31].

$$\ln\left(\frac{\beta}{T_m^2}\right) = \frac{-E_a}{RT_m} + \ln\left(\frac{K_0R}{E_a}\right) \quad (2)$$

$$\ln(\beta) = \frac{-E_a}{RT_m} + \ln\left(\frac{K_0R}{E_a}\right) \quad (3)$$

where  $\beta$  is the heating rate, As shown in Fig. 10(b), A line was placed on the Kissingers plot between  $\ln(\beta/T_m^2)$  and  $1000/T_m$ . The slope and intercept were used to compute the activation energy ( $E_a$ ) and frequency factor ( $K_0$ ), respectively. The same plot was used to calculate the correlation coefficient R-squared ( $R_2$ ). In Table 2, the values of  $E_a$ ,  $K_0$ , and  $R_2$  are shown. The activation energy of 2A4MPPP measured by the Kissinger method is 49.8074 kJ/mol. The plot of  $\ln(\beta)$  against  $1000/T_m$  denotes the Ozawa plot, shown in Fig. 10(c). The obtained slope value from this plot is used to calculate the activation energy, whose value is found to be 51.559 kJ/mol. As a result, both approaches were used to determine the activation energy needed to drive the reaction of 2A4MPPP crystal, and they were found to be quite close to one another.

The relationship between this parameter and the degree of conversion of the title compound is given in the following Equation (4) [41],

$$\alpha = \frac{M_s - M(t, T)}{M_s - M_f} \quad (4)$$

where,  $M_s$  is the initial mass,  $M_f$  is the final mass and  $M(t, T)$  is the instantaneous mass which depends on temperature and time. The plot was drawn between calculated  $\alpha$  and temperature ( $T$ ) as given in Fig. 10(d). The calculated values of conversion maxima ( $\alpha_{max}$ ) are

presented in Table 2 for all the heating rates.

### 3.5. Dielectric analysis

Dielectric constant and loss factor are the key parameters in the relevance of dielectric material-based solid-state electronic devices. A material's dielectric constant depends mainly on frequency and temperature and is primarily interrelated with the polarization of materials [42,43]. The change in a dielectric constant and dielectric loss concerning frequency in the 50 Hz - 50 MHz range are shown in Fig. 11(a) and (b) at various temperatures. The higher dielectric constant value observed at low frequencies is due to charge accumulation by interfacial or ionic polarization. It is observed that the dielectric constant values do not change for temperatures above 1 MHz. It is a well-known fact that all other polarizations except electronic polarization are eliminated at high frequencies, which means optical frequencies. The observed low dielectric loss factor in the optical frequency region confirms the occurrence of electronic polarization. Therefore, it is affirmed that the 2A4MPPP crystal has good optical quality and fewer defects.

The ac conductivity of the 2A4MPPP crystal was analyzed using the conductivity Equation (5) [44],

$$\sigma_{ac} = \epsilon_0 \epsilon_r \omega \tan \delta \tag{5}$$

When the angular frequency is  $\omega$ , absolute permittivity in free space is  $\epsilon_0$ , and phase degree is  $\delta$ . Fig. 11(c) displays the relationship between  $\ln \sigma_{ac}$  and  $\log F$  at various temperatures.

The conductivity plot shows an unexpected increase in conductivity value at high-frequency regions which could be due to relaxation in the dielectric material.

The variation of conductivity in terms of Frequency was discussed by I.B.Slima et al. [22]. The hopping energy as a function of frequency was remarkable, even though this was expected because the decrease in frequency stimulated the mobility of the free charge carriers. The density of states decreased with increasing frequency, as inferred by Mott's law, and there was also a decrease in the polaron radius. The conductivity was caused by a massive polaron. When compared to the interatomic distance, the polaron's spatial extension in this instance was substantial.

From dielectric and conductivity data, the activation energy required to initiate electrical conduction in the crystal was calculated using the Arrhenius relation (6) [45,46],

$$\sigma_T = \sigma_0 \exp(-E_a/kT) \tag{6}$$

where T is the medium's temperature,  $E_a$  is the activation energy, k is the Boltzmann constant, and  $\sigma_T$  is the medium's electrical conductivity at temperature T. Fig. 11(d) displays the  $\log \sigma_T$  with the  $1000/T$  plot (d). The activation energy  $E_a$  was determined by the linear fit approach to be 0.128 eV.

### 3.6. Mechanical behavior of 2A4MPPP

The mechanical stability of the materials is a crucial factor in employing them in device fabrication and machinery construction. Micro-indentation tests are done to know the mechanical properties such as hardness, work hardening coefficient, fracture toughness, brittleness, and stiffness. In small-scale materials, such tests are conveniently carried out using a Vickers hardness tester with a diamond indenter. This method is also called the static indentation method [46]. The Vickers hardness number (HV) of the 2A4MPPP crystal was calculated using the formula according to Equation (7) [47].

$$H_V = 1.8544 P/d^2 \text{ kg mm}^{-2} \tag{7}$$

where P is the applied load in kg, d is the indentation's diagonal length in mm, and 1.8544 is the constant for a diamond indenter with a pyramidal shape. For the title compound, the indentation duration was maintained at 10 s for each applied stress. While applying successive loads to the sample, the position of the indentation was slightly changed to avoid overlap of the indentation on the surface. The fluctuation of the hardness number with applied load is depicted in Fig. 12(a). The relation (8) was used to determine the Mohs hardness number (HM) [48], also known as scratch resistance [49], of the materials,

$$H_M = 0.675(H_V)^{1/3} \tag{8}$$

The variation of Mohs hardness with load is shown in Fig. 12(b). By Mayer's relation [42],  $p = ad^n$  (where a - constant and n - work

**Table 2**  
Thermal kinetic parameters of 2AMPPP.

Heating rate ( $\beta$ ) °C/min	$T_m$ °C	$E_a$ kJ/mol	$K_0$ $S^{-1}$	$K$ $S^{-1}$	$R^2$	$n$	$\alpha_{max}$ $min^{-1}$
5	102.8	49.8074	$4.3208 \times 10^4$	4.0762	0.8154	0.9755	0.02517
10	103.3			4.0773		0.6289	0.01941
15	104.8			4.0807		0.7261	0.01721
20	105.5			4.0822		0.4953	0.01548
25	106.5			4.0845		0.3413	0.01409

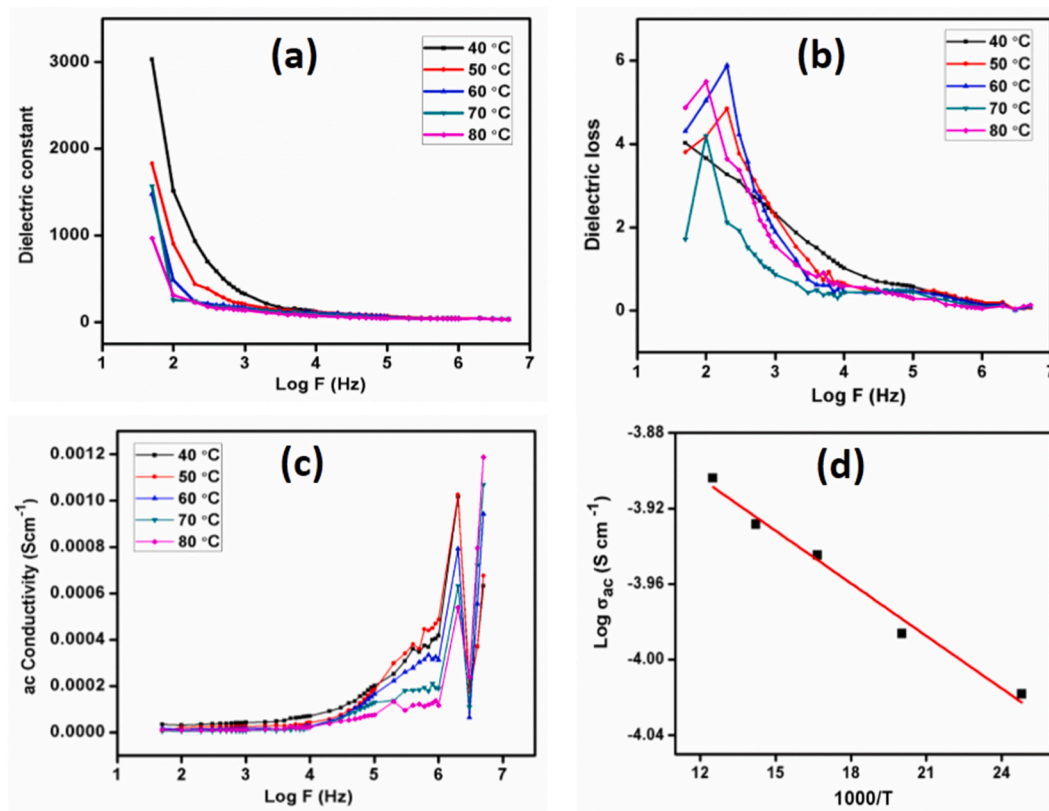


Fig. 11. (a) Frequency dependent dielectric constant, (b) Frequency dependent dielectric loss, (c) Frequency dependent ac conductivity analysis, (d) Arrhenius plot of 2A4MPPP crystal.

hardening coefficient) the work hardening coefficient was calculated.

The work hardening coefficient is the slope value determined by the linear fitting of the log P against the log D plot (Fig.12(c)) (n). The number n is discovered to be 3.416, which suggests that the substance is soft. Hays and Kendall [50] introduced the load-dependence hardness equation as  $P = W + A_1 d^2$ , where W is the minimum stress required to cause plastic deformation and A1 is constant. Fig. 12(d) displays a plot of log D vs log(P-W). From the plot, the work hardening coefficient (n) value was obtained as 3.438.

Fracture toughness strongly depends on the crack length and the type of crack observed during indentation. At the corners of the indentation, cracks developed due to the application of load onto the sample's surface. The c/a ratio (where, c is the crack length and a is half the diagonal length of the indenter) is an indicator of the nature of the crack. If  $c/a \geq 2.5$ , it means the half penny or median crack and if  $c/a < 2.5$ , it represents the palmqvist crack type [51]. The c/a ratio of the 2A4MPPP crystal was found to be 2.02. Thus, the 2A4MPPP crystal is the palmqvist crack type. By using the empirical relation (9), the fracture toughness (Kc) of a 2A4MPPP crystal with a palmqvist crack system was determined [52],

$$K_c = \frac{P}{\beta_0 a l^{1/2}} \quad (9)$$

where,  $\beta_0 = 7$  for Vickers micro indenter and  $l = c-a$ , the fracture toughness value was calculated to be  $45.62 \text{ Mkgmm}^{-3/2}$ . Another important mechanical parameter is brittleness caused by plastic flow and densification in the material [53].

Using Equation (10), the brittleness index ( $B_i$ ) was estimated to be  $0.483 \times 10^3 \text{ m}^{-1/2}$  [54],

$$B_i = H_v / K_c \quad (10)$$

From relations (9) and (10), it is understood that the crack initiation load plays a crucial role in the fragility of the sample. Thus, the formula was used to estimate the stiffness constant of the compound in the title [55],  $C_{11} = H_v^{7/4}$ . The variation of stiffness constant with load is shown in Fig. 12(e).

#### 4. Conclusion

In conclusion, for the first time, the 2-amino 4-methylpyridinium 4-nitrophenolate 4-nitrophenol bulk single crystal has been successfully grown in the Bridgman technique using a single wall ampoule. This work was motivated by an interest in growing

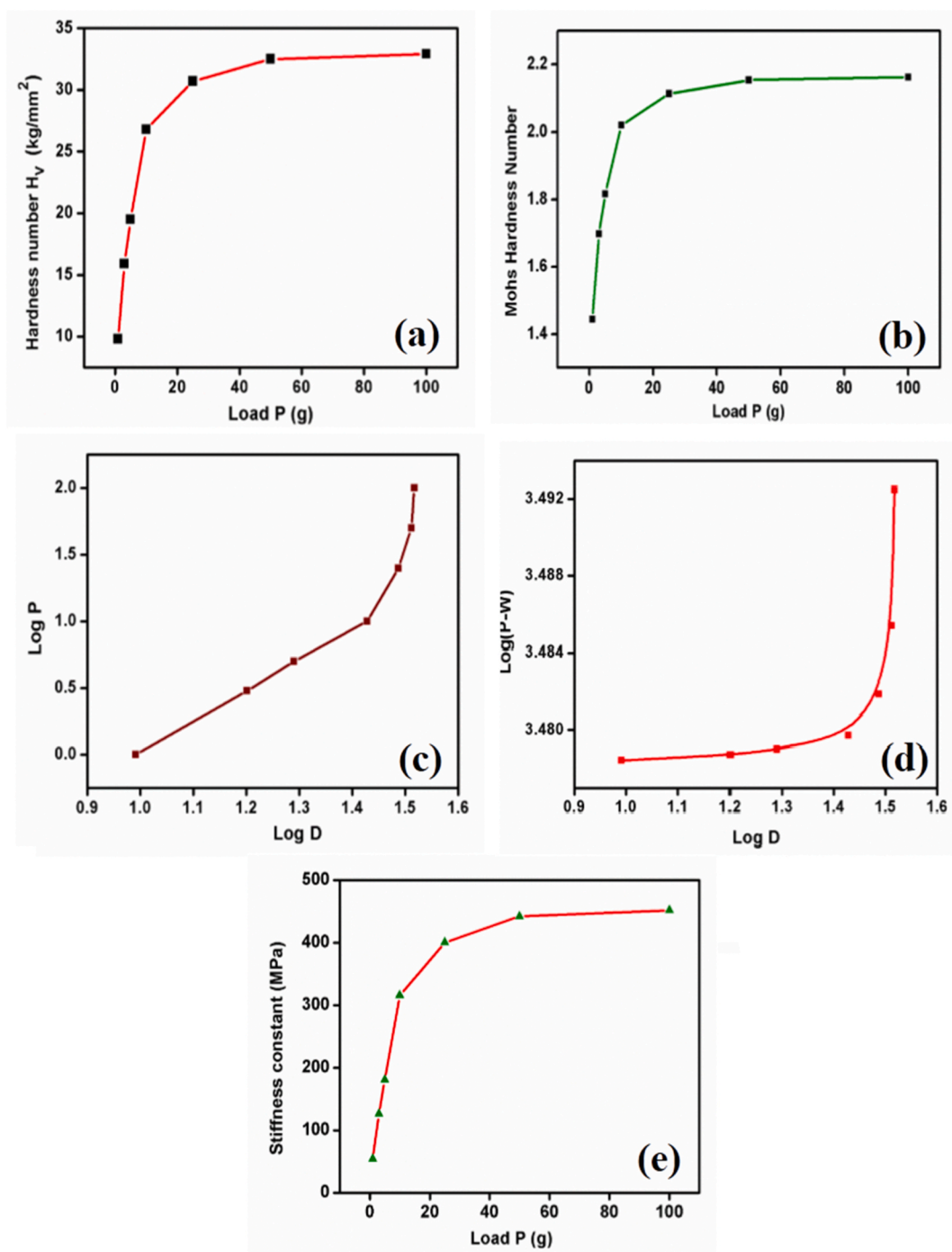


**Fig. 12.** (a) Variation of Hardness number with load, (b) Variation of Mohs hardness number with load, (c) plot of Log D versus Log P, (d) plot of Log(P-W) versus Log D, (e) Variation of stiffness constant with load.

thermally and mechanically stable bulk single crystals for device applications. By using X-ray diffraction to determine the crystal's structure, it was discovered that it is an orthorhombic crystal system with the space group Pna21. By using <sup>1</sup>H-NMR and FT-IR spectroscopic research has confirmed that the chemical structure and vibrational modes of the various functional groups present in the crystal are correct. The crystal's melting point is somewhere around 103 °C, according to the results of TGA and DTA analysis. The crystal's purity and perfection are indicated by its endothermic peak. The crystal's low dielectric constant and high-frequency dielectric loss are shown by the dielectric investigations. According to Vickers microhardness investigations, grown 2A4MPPP falls under the category of soft materials. As soon as the crystal was loaded, a Palmquist-type crack was seen. The value determined for the

work hardening coefficient ( $n$ ) was 3.438, which is close to the result of Mayer's equation. Further assessed were the Mohs hardness number, fracture toughness, brittleness index, and stiffness constant. The 2A4MPPP crystal's distinguishing characteristics and attributes suggest that it might be a good material for electromechanical, thermomechanical, and electro-optical applications.

### Author contribution statement

S. Karuppusamy, S. Muralidharan, K. Dinesh Babu: conceived and designed the experiments; performed the experiments; Analyzed and interpreted the data; Contributed reagents, materials, analysis tools or data; wrote the paper. P. Sakthivel, Dongjin Choi: Performed the experiments; contributed reagents, materials, analysis tools or data; wrote the paper.

### Data availability statement

Data will be made available on request.

### Declaration of competing interest

The authors declare that they have no known competing financial interests or personal relationships that could have appeared to influence the work reported in this paper.

### Acknowledgements

This research work was supported by the International Science & Business Belt support program, through the Korea Innovation Foundation funded by the Ministry of Science and ICT (No:2023-SB-SB-0105-01-101).

The authors would like to dedicate this work to Late Dr. R. Gopalakrishnan, Department of Physics, Anna University, Chennai - 600 025. The authors are thankful to SAIF - IIT Madras for instrumentation facility and also thank to Dr. P. Vijayakumar, Materials Science Group, Indira Gandhi Centre for Atomic Research, Kalpakkam, 603102, India. for his fruitful discussions.

### References

- [1] M. Arivanandhan, X. Huang, S. Uda, G. Bhagavannarayana, N. Vijayan, K. ankanarayanan, P. Ramasamy, Directional growth of organic NLO crystal by different growth methods: a comparative study by means of XRD, HRXRD and laser damage threshold, *J. Cryst. Growth* 310 (2008) 4587–4592, <https://doi.org/10.1016/j.jcrysgro.2008.08.036>.
- [2] B. Teng, J. Wang, Z. Wang, X. Hu, H. Jiang, H. Liu, X. Cheng, S. Dong, Y. Liu, Z. Shao, Crystal growth, thermal and optical performance of BiB<sub>3</sub>O<sub>6</sub>, *J. Cryst. Growth* 233 (2001) 282–286, [https://doi.org/10.1016/S0022-0248\(01\)01526-3](https://doi.org/10.1016/S0022-0248(01)01526-3).
- [3] P. Preeda, R. Ganapathi Raman, P. Sakthivel, FTIR Structural, FT-Raman, optical and nonlinear optical properties of organic nonlinear optical crystal –3,5-diisopropyl-2-hydroxybenzoic acid, *Inorganic Chemistry Communications* 146 (2022) 110120, <https://doi.org/10.1016/j.inoche.2022.110120>.
- [4] J. Takeya, M. Yamagishi, Y. Tominari, R. Hirahara, Y. Nakazawa, T. Nishikawa, T. Kawase, T. Shimoda, S. Ogawa, Very high-mobility organic single-crystal transistors with in-crystal conduction channels, *Appl. Phys. Lett.* 90 (2007), 102120, <https://doi.org/10.1063/1.2711393>.
- [5] N. Suresh, M. Selvapandian, P. Sakthivel, K. Loganathan, Structural, optical, thermal, and magnetic properties of strontium nitrate doped l-Alanine crystal, *Optik* 221 (2020) 165336, <https://doi.org/10.1016/j.ijleo.2020.165336>.
- [6] R.J. Vijay, N. Melikechi, T. Thomas, R. Gunaseelan, M.A. Arockiaraj, P. Sagayaraj, Investigation on the growth of DAST crystals of large surface area for THz applications, *Mater. Chem. Phys.* 132 (2012) 610–617, <https://doi.org/10.1016/j.matchemphys.2011.11.076>.
- [7] Z.M. Jin, Y.J. Pan, D.J. Xu, Y.Z. Xu, The 1:1 complex of 4-nitrophenol and 4-methylpyridine, *Acta Crystallogr. C* 56 (2000) e69–e70, <https://doi.org/10.1107/S0108270100001074>.
- [8] T. Suthan, P.V. Dhanaraj, N.P. Rajesh, C.K. Mahadevan, G. Bhagavannarayana, Growth and characterization of benzil single crystals using nanotranslation by the modified vertical Bridgman technique, *CrystEngComm* 13 (2011) 4018–4024, <https://doi.org/10.1039/C0CE00453G>.
- [9] H. Chen, P. Yang, C. Zhou, C. Jiang, J. Pan, Growth of LaCl<sub>3</sub>:Ce<sup>3+</sup> crystal by the vertical bridgman process in a nonvacuum atmosphere, *Cryst. Growth Des.* 6 (2006) 809–811, <https://doi.org/10.1021/cg050358c>.
- [10] G. Zhang, H. Ruan, X. Zhang, S. Wang, X. Tao, Vertical Bridgman growth and optical properties of CdSiP<sub>2</sub> crystals, *CrystEngComm* 15 (2013) 4255–4260, <https://doi.org/10.1039/C3CE27003C>.
- [11] B.C. Houchens, P. Becla, S.E. Tritchler, A.J. Goza, D.F. Bliss, Crystal growth of bulk ternary semiconductors: comparison of GaInSb growth by horizontal Bridgman and horizontal traveling heater method, *J. Cryst. Growth* F312 (2010) 1090–1094, <https://doi.org/10.1016/j.jcrysgro.2009.12.051>.
- [12] A. Krishna, N. Vijayan, C. Bagdia, K. Thukral, D. Haranath, K.K. Maurya, G. Bhagavannarayana, Effect of ampoule support on the growth of organic benzimidazole single crystals by vertical Bridgman technique for nonlinear optical applications, *CrystEngComm* 18 (2016) 4844–4850, <https://doi.org/10.1039/C6CE000891G>.
- [13] S. Karuppusamy, K. Dinesh Babu, P. Sakthivel, Evaluation of thermal, dielectric and mechanical behavior of 4-nitrophenol crystal, *Chemical Physics Letters* 807 (2022) 140098, <https://doi.org/10.1016/j.cplett.2022.140098>.
- [14] V. Krishnakumar, M. Rajaboopathi, R. Nagalakshmi, Studies on vibrational, dielectric, mechanical and thermal properties of organic nonlinear optical co-crystal: 2,6-diaminopyridinium-4-nitrophenolate-4-nitrophenol, *Physica B* 407 (2012) 1119–1123, <https://doi.org/10.1016/j.physb.2012.01.084>.
- [15] T. Chen, Z. Sun, L. Li, S. Wang, Y. Wang, J. Luo, M. Hong, Growth and characterization of a nonlinear optical crystal—2,6-diaminopyridinium 4-nitrophenolate 4-nitrophenol (DAPNP), *J. Cryst. Growth* 338 (2012) 157–161, <https://doi.org/10.1016/j.jcrysgro.2011.10.023>.
- [16] G.A. Babu, R.P. Ramasamy, P. Ramasamy, Synthesis, crystal growth and characterization of an efficient nonlinear optical D–π–A type single crystal: 2-Aminopyridinium 4-nitrophenolate 4-nitrophenol, *Mater. Chem. Phys.* 117 (2009) 326–330, <https://doi.org/10.1016/j.matchemphys.2009.06.011>.
- [17] P. Srinivasan, T. Kanagasekaran, N. Vijayan, G. Bhagavannarayana, R. Gopalakrishnan, P. Ramasamy, Studies on the growth, optical, thermal and dielectric aspects of a proton transfer complex – dimethyl amino pyridinium 4-nitrophenolate 4-nitrophenol (DMAPNP) crystals for non-linear optical applications, *Opt. Mater.* 30 (2007) 553–564, <https://doi.org/10.1016/j.optmat.2007.01.014>.
- [18] S. Muralidharan, P. Nagapandiselvi, T. Srinivasan, Y. Vidyalakshmi, D. Velmurugan, R. Gopalakrishnan, Synthesis, growth, spectral and computational studies on aminomethylpyridinium trichloro acetate single crystal, *Chin. J. Phys.* 73 (2021) 746–755, <https://doi.org/10.1016/j.cjph.2021.08.010>.
- [19] T. Chen, Z. Sun, C. Song, Y. Ge, J. Luo, W. Lin, M. Hong, Bulk crystal growth and optical and thermal properties of the nonlinear optical crystal l-Histidinium-4-nitrophenolate 4-nitrophenol (LHPP), *Cryst. Growth Des.* 12 (2012) 2673–2678, <https://doi.org/10.1021/cg300262t>.

- [20] I.B. Slima, K. Karoui, A.B. Rhaïem, Ionic conduction, structural and optical properties of LiCoO<sub>2</sub> compound, *Ionics* 29 (2023) 1731–1739, <https://doi.org/10.1007/s11581-023-04960-w>.
- [21] K. Trabelsi, K. Karoui, F. Hajlaoui, M. Zaghrouri, F. Jomni, A.B. Rhaïem, An organic-inorganic hybrid cadmium chloride with face-sharing CdCl<sub>6</sub> octahedral chains: synthesis, crystal structure, optical and conduction mechanisms: [NH<sub>2</sub>(CH<sub>3</sub>)<sub>2</sub>SCd<sub>3</sub>Cl<sub>11</sub>], *Opt. Mater.* 134 (2022), 113100, <https://doi.org/10.1016/j.optmat.2022.113100>.
- [22] I.B. Slima, K. Karoui, A. Mahmoud, F. Boschini, A.B. Rhaïem, *RSC Adv.* 12 (2022) 1563, <https://doi.org/10.1039/D1RA08263A>.
- [23] P. Karuppasamy, T. Kamalesh, K. Anitha, S. Abdul Kalam, Muthu Senthil Pandian, P. Ramasamy, Sunil Verma, S. Venugopal Rao, 2-Amino 4-methylpyridinium 3-chlorobenzoate – a phase matchable organic nonlinear optical material for optoelectronics device applications, *Opt. Mater.* 84 (2018) 475–489, <https://doi.org/10.1016/j.optmat.2018.07.039>.
- [24] B. Babu, J. Chandrasekaran, R. Thirumurugan, K. Anitha, M. Saravanabhavan, 2-Amino 4-methylpyridinium 3-chlorobenzoate – a phase matchable organic nonlinear optical material for optoelectronics device applications, *Opt. Laser. Technol.* 94 (2017) 253–260, <https://doi.org/10.1016/j.optlastec.2017.04.007>.
- [25] M. Saravanakumar, J. Chandrasekaran, M. Krishnakumar, B. Babu, B. Mohanbabu, G. Vinitha, Growth, spectral and quantum chemical investigation on hexamethylenetetramine 4-nitrophenol monohydrate single crystals for second harmonic generation and optical limiting applications, *J. Mol. Struct.* 1265 (2022), 133406, <https://doi.org/10.1016/j.molstruc.2022.133406>.
- [26] R. Kaliammal, G. Parvathy, G. Maheshwaran, V. Kousalya Devi, M. Krishna Kumar, K. Sankaranarayanan, S. Sudhakar, Experimental and theoretical studies on new 2-amino-6-methylpyridinium 2,4-dihydroxybenzoate monohydrate organic single crystal for second order nonlinear optical applications, *J. Mol. Struct.* 1254 (2022), 132330, <https://doi.org/10.1016/j.molstruc.2022.132330>.
- [27] K. Venkatesan, M. Kayalvizhi, L. Jothi, G. Vasuki, Growth, structural, optical, Z-scan and dielectric analysis of 2-Amino-4-methylpyridinium 2-chloro 4-nitro benzoate crystals for third order non-linear optical applications, *J. Mol. Struct.* 1258 (2022), 132687, <https://doi.org/10.1016/j.molstruc.2022.132687>.
- [28] T. Murugan, S. Suresh, B. Milton Boaz, Studies on the growth and characterization of a new organic nonlinear optical single crystal: 2-amino 5-methylpyridinium 4-methoxybenzoate for optoelectronic and photonic devices, *Opt. Mater.* 136 (2023), 113379, <https://doi.org/10.1016/j.optmat.2022.113379>.
- [29] B.R. Krishnamoorthy, S. Kannan, K. Sivaperuman, Synthesis and crystal growth of 2, 3-dimethyl-N-[2-(hydroxy) benzylidene] aniline: an organic second-order non-linear optical crystal for non-linear optical (NLO) applications, *Opt. Mater.* 113 (2021), 110864, <https://doi.org/10.1016/j.optmat.2021.110864>.
- [30] R. Kaliammal, G. Parvathy, G. Maheshwaran, K. Sankaranarayanan, M. Arivanandhan, S. Sudhakar, Crystal growth, structural, optical, thermal, and mechanical properties of new bis(2-amino-6-methyl pyridinium barbiturate) tetrahydrate organic single crystal for nonlinear optical applications, *Chin. J. Phys.* 68 (2020) 436–460, <https://doi.org/10.1016/j.cjph.2020.09.027>.
- [31] M. Fatmi, B. Ghebouli, M.A. Ghebouli, T. Chihhi, M. Abdul Hafiz, The kinetics of precipitation in Al-2.4 wt% Cu alloy by Kissinger, Ozawa, Bosswel and Matusita methods, *Phys. B Condens. Matter* 406 (2011) 2277–2280, <https://doi.org/10.1016/j.physb.2011.03.053>.
- [32] Y.C. Liu, L.S. Chao, Extra nodes added on the solid/liquid interface to solve the mass transfer problem in a directional solidification process, *Mater. Trans.* 48 (2007) 2289–2296, <https://doi.org/10.2320/matertrans.MB200711>.
- [33] M. Arivanandhan, K. Sankaranarayanan, K. Ramamoorthy, C. Sanjeeviraja, P. Ramasamy, Growth of organic single crystals by transparent vertical Bridgman technique and its characterization, *Thin Solid Films* 477 (2005) 2–6, <https://doi.org/10.1016/j.tsf.2004.08.162>.
- [34] P.S. Dutta, K.S. Sangunni, H.L. Bhat, V. Kumar, Growth of gallium antimonide by vertical Bridgman technique with planar crystal-melt interface, *J. Cryst. Growth* 141 (1994) 44–50, [https://doi.org/10.1016/0022-0248\(94\)90090-6](https://doi.org/10.1016/0022-0248(94)90090-6).
- [35] A. Zappettini, M. Zha, L. Marchini, D. Calestani, Control of the interface shape in vertical Bridgman grown CdZnTe crystals for X-ray detector applications, *CrystEngComm* 14 (2012) 5992–5995, <https://doi.org/10.1039/C2CE25452B>.
- [36] M.P. Volz, K. Mazuruk, Existence and shapes of menisci in detached Bridgman growth, *J. Cryst. Growth* 321 (2011) 29–35, <https://doi.org/10.1016/j.jcrysgro.2011.02.035>.
- [37] C. Stelian, M.P. Volz, J.J. Derby, On favorable thermal fields for detached Bridgman growth, *J. Cryst. Growth* 311 (2009) 3337–3346, <https://doi.org/10.1016/j.jcrysgro.2009.03.043>.
- [38] D. Schulz, S. Ganschow, D. Klimm, K. Struve, Inductively heated Bridgman method for the growth of zinc oxide single crystals, *J. Cryst. Growth* 310 (2008) 1832–1835, <https://doi.org/10.1016/j.jcrysgro.2007.11.050>.
- [39] J. Baram, V. Erukhimovitch, Application of thermal analysis methods to nucleation and growth transformation kinetics, Part II, *Thermochim. Acta* 323 (1998) 43–51, [https://doi.org/10.1016/S0040-6031\(98\)00505-X](https://doi.org/10.1016/S0040-6031(98)00505-X).
- [40] E. Benavidez, L. Santini, E. Brandaleze, Decomposition kinetic of carbonaceous materials used in a mold flux design, *J. Therm. Anal. Calorim.* 103 (2011) 485–493, <https://doi.org/10.1007/s10973-010-1081-5>.
- [41] O. Kaygili, Synthesis and characterization of Na<sub>2</sub>O–CaO–SiO<sub>2</sub> glass–ceramic, *J. Therm. Anal. Calorim.* 117 (2014) 223–227, <https://doi.org/10.1007/s10973-014-3655-0>.
- [42] B.M. Boaz, B. Varghese, C.J. Raj, S.J. Das, Growth, microhardness, dielectric and photoconductivity studies on NPNaLi: a promising crystal for NLO applications, *Mater. Sci. Eng. B* 136 (2007) 57–61, <https://doi.org/10.1016/j.mseb.2006.09.003>.
- [43] R. Hanumantharao, S. Kalainathan, Growth, spectroscopy, dielectric and nonlinear optical studies of novel organic NLO crystal: l-Threonine formate, *Spectrochim. Acta, Part A* 94 (2012) 78–83, <https://doi.org/10.1016/j.saa.2012.03.062>.
- [44] P. Krishnan, K. Gayathri, N. Sivakumar, S. Gunasekaran, G. Anbalagan, Nucleation kinetics, growth, crystalline perfection, mechanical, thermal, optical and electrical characterization of brucinium 2-carboxy-6-nitrophthalate dihydrate single crystal, *J. Cryst. Growth* 396 (2014) 85–94, <https://doi.org/10.1016/j.jcrysgro.2014.03.044>.
- [45] M.B. Bechir, A.B. Rhaïem, K. Guidara, A.c. conductivity and dielectric study of LiNiPO<sub>4</sub> synthesized by solid-state method, *Bull. Mater. Sci.* 37 (2014) 473–480, <https://doi.org/10.1007/s12034-014-0685-y>.
- [46] M. Okutan, E. Basaran, H.I. Bakan, F. Yakuphanoglu, AC conductivity and dielectric properties of Co-doped TiO<sub>2</sub>, *Physica B* 364 (2005) 300–305, <https://doi.org/10.1016/j.physb.2005.04.027>.
- [47] M.E. Broz, R.F. Cook, D.L. Whitney, Microhardness, toughness, and modulus of Mohs scale minerals, *Am. Mineral.* 91 (2006) 135–142, <https://doi.org/10.2138/am.2006.1844>.
- [48] T.S. Shyju, S. Anandhi, R. Gopalakrishnan, Comparative studies on conventional solution and Sankaranarayanan–Ramasamy (SR) methods grown potassium sodium tartrate tetrahydrate single crystals, *CrystEngComm* 14 (2012) 1387–1396, <https://doi.org/10.1039/C1CE05849E>.
- [49] D. Yuan, Z. Jia, J. Wang, Z. Gao, J. Zhang, X. Fu, J. Shu, Y. Yin, Q. Hu, X. Tao, Bulk growth, structure, and characterization of the new monoclinic TbCa<sub>4</sub>(BO<sub>3</sub>)<sub>3</sub> crystal, *CrystEngComm* 16 (2014) 4008–4015, <https://doi.org/10.1039/C4CE00051J>.
- [50] H. Yang, F. Peng, Q. Zhang, C. Guo, C. Shi, W. Liu, G. Sun, Y. Zhao, D. Zhang, D. Sun, S. Yin, A promising high-density scintillator of GdTaO<sub>4</sub> single crystal, *CrystEngComm* 16 (2014) 2480–2485, <https://doi.org/10.1039/C3CE42350F>.
- [51] K. Sangwal, On the reverse indentation size effect and microhardness measurement of solids, *Mater. Chem. Phys.* 63 (2000) 145–152, [https://doi.org/10.1016/S0254-0584\(99\)00216-3](https://doi.org/10.1016/S0254-0584(99)00216-3).
- [52] K. Sangwal, B. Surowska, P. Błaziak, Relationship between indentation size effect and material properties in the microhardness measurement of some cobalt-based alloys, *Mater. Chem. Phys.* 80 (2003) 428–437, [https://doi.org/10.1016/S0254-0584\(02\)00546-1](https://doi.org/10.1016/S0254-0584(02)00546-1).
- [53] B. Lal, K.K. Bamzai, P.N. Kotru, B.M. Wanklyn, Microhardness, fracture mechanism and dielectric behaviour of flux-grown GdFeO<sub>3</sub> single crystals, *Mater. Chem. Phys.* 85 (2004) 353–365, <https://doi.org/10.1016/j.matchemphys.2004.01.013>.
- [54] J. Sehgal, S. Ito, Brittleness of glass, *J. Non-Cryst. Solids* 253 (1999) 126–132, [https://doi.org/10.1016/S0022-3093\(99\)00348-8](https://doi.org/10.1016/S0022-3093(99)00348-8).
- [55] K. Sangwal, Review: indentation size effect, indentation cracks and microhardness measurement of brittle crystalline solids – some basic concepts and trends, *Cryst. Res. Technol.* 44 (2009) 1019–1037, <https://doi.org/10.1002/crat.200900385>.